

On-chip optical processing

M. Edward Motamedi

Rockwell Science Center

1049 Camino Dos Rios, Thousand Oaks, CA 91360

Ming C. Wu and Kristofer S.J. Pister

Department of Electrical Engineering, University of California, Los Angeles

405 Hilgard Avenue, Los Angeles, CA 90095

ABSTRACT

Microoptical components, such as diffractive and refractive microlenses, micromirrors, beam splitter and beam combining have recently received considerable attention in the optics R&D centers and finally in the manufacturing community. This achievement is due to MEM technology that demonstrated major improvements in overall performance/cost of optical systems while offering the possibility of relatively rapid transition to products for military, industrial and consumer markets. Because of these technology advances, an industrial infrastructure is rapidly becoming established to provide combining microoptical components and MEM-based microactuators for on-chip optical processing. Optical systems that once were considered to be impractical due to the limitations of bulk optics can now easily be designed and fabricated with all required optical paths, signal conditioning, and electronic controls, integrated on a single chip. On-chip optical processing will enhance the performance of devices such as focal plane optical concentrator, smart actuators, color separation, beam shaping, FDDI switch, DMDs, and miniature optical scanners. In this paper we review advances in microoptical components developed at Rockwell Science Center. We also review the potential of on-chip optical processing and recent achievement of free-space integrated optics and microoptical bench components developed at UCLA, and digital micromirror devices (DMDs) developed at Texas Instruments.

Keywords: MEMS, microoptics, MOEM, actuators, integration, mirror, microlens, DMDs, FDDI, digital video

1. INTRODUCTION

Microoptical components, such as diffractive and refractive microlenses, have recently received considerable attention for development of optical systems¹⁻⁵. Achievements in microoptical functions such as focal plane optical concentration,^{6,1,2} optical efficiency enhancement, digital video development, color separation, and beam shaping and transforming,⁷ have demonstrated the potential of this technology. In the first generation of the miniaturized optical system, microoptical components were hybridized with electronics circuits and in some cases with movable components such as scanning mirrors and piezo-actuators. As microelectronic technology advanced by novel

development in micromachining and micro-electro-mechanical (MEM) technology, miniaturized optical systems also advanced to nearly complete monolithic systems.

MEM technology combines mechanical structures with electronics to perform mechanical motions offering a host of actuators and wide applications in optical systems. Merging microoptics, microelectronics and micromechanics creates a new and broader class of micro-opto-electro-mechanical (MOEM) devices,^{8,9} which may attract additional industrial demonstrations of commercial devices. A few examples are torsional mirrors, digital micromirror devices (DMDs), laser scanners, fiber data distribution interface (FDDI), 3-D tunable Fabry-Perot etalons, optical shutters, MEM optical switches, optical interconnection, data storage, and MEM corner cube reflectors. Integrated devices based on MOEM systems can form free space integrated optics and consequently push technology to the development of a microoptical bench on a chip.

In this paper, we first review recent developments and achievement in microoptics (section 2), and microoptical MEM and on-chip optical processing (section 3). In section 3, we discuss the development of microoptical bench and free space interconnections¹⁰⁻¹⁴. Then we introduce several applications of optical MEM devices with the potential of on-chip optical processing (section 4). Section 4 includes major topics of on-chip optical processing. We discuss in detail development of 3-D tunable Fabry-Perot,¹⁵⁻¹⁹ FDDI optical bypass switch,²⁰⁻²² MEM corner cube reflector,²³ digital display using DMDs,²⁴⁻²⁹ and, finally, optical scanners³⁰.

2. MICROOPTICS

Microoptics technology is becoming increasingly essential to the development of many dual use optical systems. Optical components such as diffractive and refractive microlenses,¹⁻⁵ multilevel optical grating, beam splitter, and optical transformer,⁷ are being incorporated into advanced military sensor systems and commercial products. Microoptics is an enabling technology for applications that cannot be addressed using conventional optics. In the following we will discuss some of these microcomponents as subtechnologies of microoptics.

2.1 Diffractive microlenses

The first breakthrough in optical processing was the development of diffractive microlenses. A diffractive microlens is a microoptical component with dimension as small as a few tens of μm in diameter and a thickness on the order of the optical wavelengths. The microlens speed can be as fast as $F/0.3$ in air for high index materials such as silicon and GaAs¹ and about $F/1$ for quartz and glass substrates. A diffractive microlens is an approximation of a kinoform lens. A kinoform lens or a continuous diffractive lens is defined by applying a phase function constraint between 0 and 2π to subtract the integral numbers of wavelengths from the lens transmittance function. Theoretically, a kinoform lens has 100% diffraction efficiency. The kinoform lens structure can be approximated by a multilevel lithography and stepwise etching. To fabricate a multistep process, binary optic design is considered. Binary optics will reduce the number of lithographic masks by a factor of $2^m/m$, where m is the number of required masks.

For binary optic structure, the phase transmittance is quantized with the phase step heights defined by the relation (1).

$$d(m) = \frac{\lambda}{(n-1)2^m} \quad (1)$$

where λ is the light wavelength in free space, n is the index of refraction of the lens material, m is the mask number for level m process and $d(m)$ is the etch depth of the level m . An m -mask process produces an $M = 2^m$ step approximation to a continuous blazed diffractive structure. The efficiency of the incident energy diffracted into the first order is given by,

$$\eta = \left[\frac{\sin\left(\frac{\pi}{M}\right)}{\left(\frac{\pi}{M}\right)} \right]^2 \quad (2)$$

For $M = 4, 8, \text{ or } 16$, $\eta = 0.81, 0.95, \text{ or } 0.99$, respectively.

Since microlenses operate over a small range in incident angle, a simple planar thin film lens design is acceptable. The optical path difference (OPD) function for each lens is used to derive the following relationship among the zone radius, focal length, and wavelength.²

$$r(p,m) = \sqrt{\left(\frac{p\lambda}{n2^m}\right)^2 + 2f\left(\frac{p\lambda}{n2^m}\right)} \quad (3)$$

where f is the focal length, $p = 0,1,2,3,\dots$, n is the refractive index of the substrate and $r(p, m)$ is the successive zone radii for the patterns in mask number m .

Figure 1 shows a processing cycle for fabrication of an eight-level binary optic microlens. Figures 1(a), 1(b) and 1(c) illustrate the process of two-phase, four-phase and eight-phase microlenses where the etch depth and zone radii of each process can be determined from expression (1) and (3) for $m = 1, 2 \text{ and } 3$ respectively.

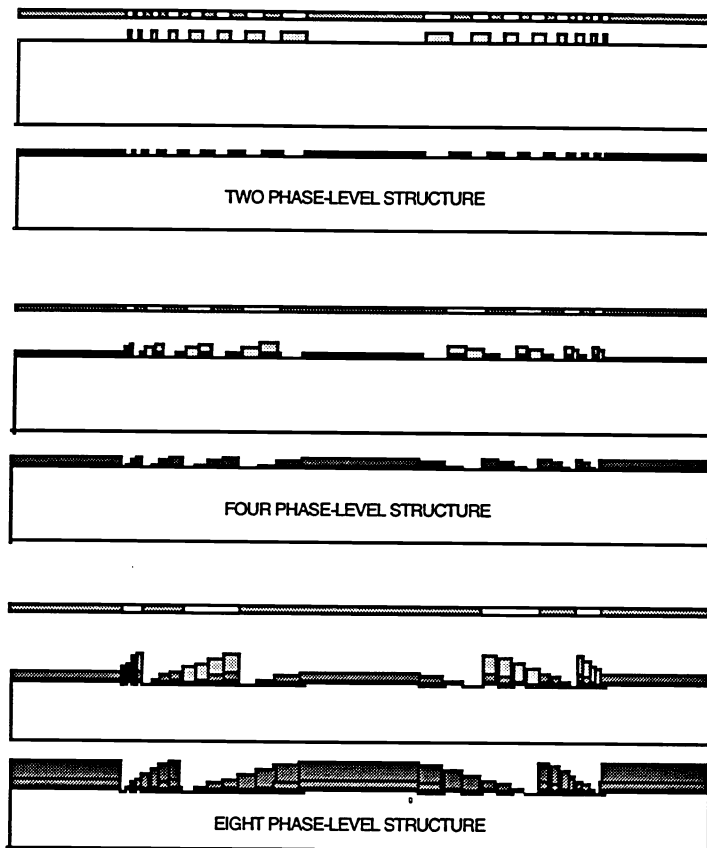


Fig. 1. Processing cycle of an eight phase-level binary optics microlens.

Binary optics can produce microlenses and lens arrays with submicron features, located and packed precisely together, with an accuracy of a fraction of a micron. Binary optics microlenses with multilevel relief structures can produce diffraction efficiency higher than 90%, which enables design of many complex optical systems not possible with bulk optics. Recently, this technology has demonstrated high quality microlens arrays, which attracted many applications in both passive and active optical sensors.^{1,2}

Three independent optical and processing parameters that are important in the design of a binary optic microlens are wavelength, λ ; F/number (F#); and the smallest process feature size or critical dimension, CD. The F# is equal to f/d where f is the focal length and d is the microlens diameter. For a typical eight-phase level binary optic microlens the CD value is:

$$CD = \lambda F\# / 4, \quad (4)$$

In most production laboratories the minimum VLSI feature size is 0.5 to 1 μm . This limits the binary optic microlens speed to between F/6 and F/3 for wavelengths from 0.632 μm (HeNe laser) to 0.850 μm (typical laser diode), respectively. Figure 2 shows an F/6 quartz microlens array designed for $\lambda = 0.632 \mu\text{m}$ with microlens diameter of 200 μm and 100% fill factor.

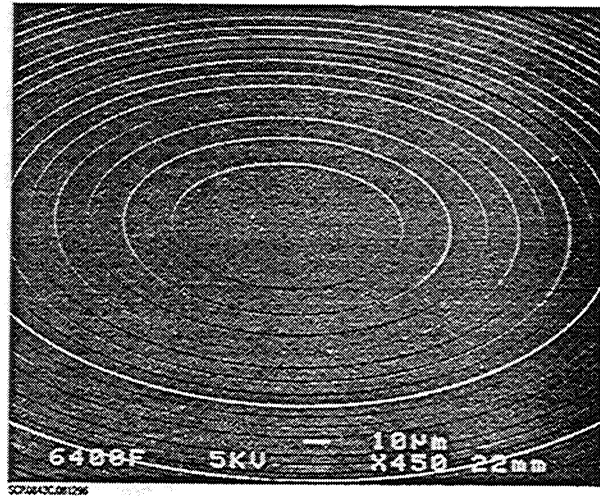


Fig. 2. SEM microphotograph of a centerzone of a F/6 quartz microlens designed for $\lambda = 0.632 \mu\text{m}$ with microlens diameter of 200 μm and 100% fill factor

According to Eq. (4), higher speed (lower F/#) microlenses can be fabricated for infrared applications. Figure 3 shows an SEM view of an F/0.6 microlens designed for 1–10 μm with microlens diameter of 240 μm and 100% fill factor.

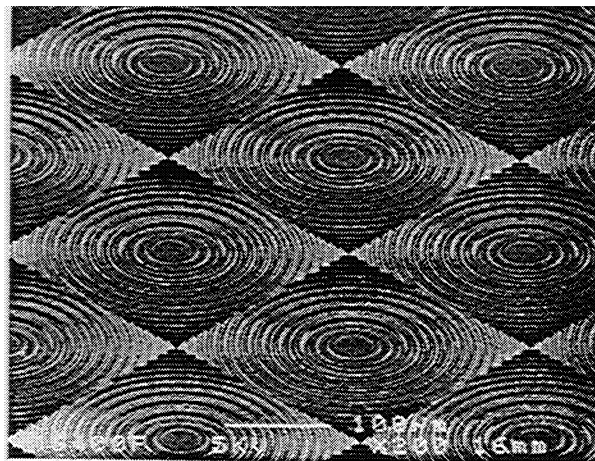


Fig. 3. SEM view of an F/0.6 microlens designed for 1–10 μm with microlens diameter of 240 μm and 100% fill factor.

An important consideration for diffractive microlenses is the diffraction efficiency. The efficiency with which the light is diffracted to the first order focus increases with the number of phase levels (see Eq. (2)). In practice, the efficiency is reduced by a number of processing factors. Values of 90% have been achieved for 8-phase-level microlenses. The extent to which this is acceptable will depend on the application.

A major feature of diffractive microlenses is the planar nature of the structure. The surface relief is on the order of the design wavelength. This will reduce the volume and weight of the optics in a typical system relative to an all-refractive design. Diffractive optical devices can be made either directly in the substrate by reactive ion etching (RIE)^{1,2} or formed on the surface by thin film deposition and lift-off techniques.^{3,6}

The advantage of using thin film deposition to fabricate binary optic microlenses is the finer control that can be applied to film thickness than to etch depth control for the RIE process. This will increase the diffraction efficiency of the device assuming all the other process parameters remain unchanged. A further advantage of this thin film deposition method is the ability to generate microlenses using materials that are not easily processed by RIE.³

The design considerations for deposited microlenses are identical to those used for RIE processed microlenses. Identical mask sets can be used for both processes. Motamedi et al. have demonstrated a single material deposition and lift-off method.³ This work also emphasizes submicron process and technology trade-offs between standard RIE and thin film deposited binary optics microlens arrays. The process steps of the thin film deposition method are shown in Fig. 4.

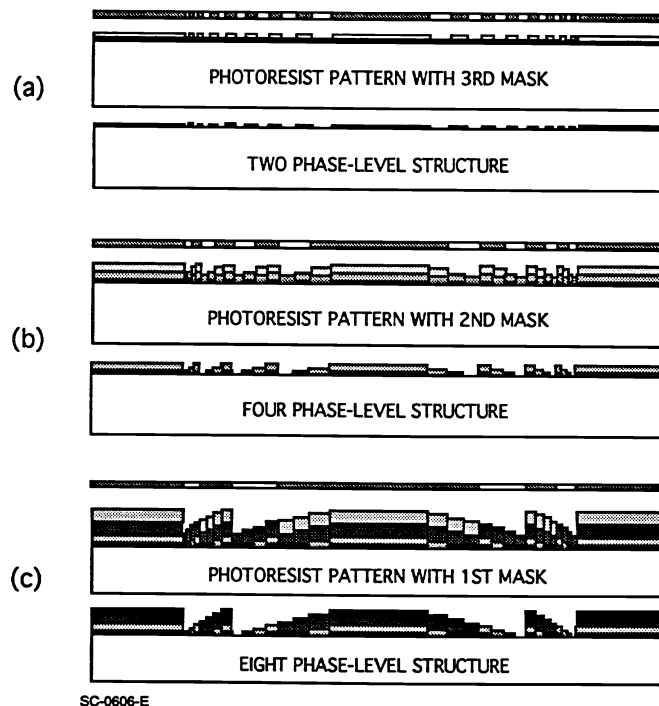


Fig. 4. A typical profile of an 8-level thin film binary optic microlens processed by projection lithography.

One approach to this process is to use an image reversal photoresist, which has the advantage of producing a negative slope pattern, a crucial requirement for submicron lift-off processing. An example of the use of the thin film method to generate microlenses in a material that is not readily processed using RIE is an all-sapphire (Al_2O_3) microlens array. Figure 5 is an SEM photomicrograph of an eight-phase level F/17 thin film microlens. The optical quality of these microlenses was evaluated by measuring the point spread function.³

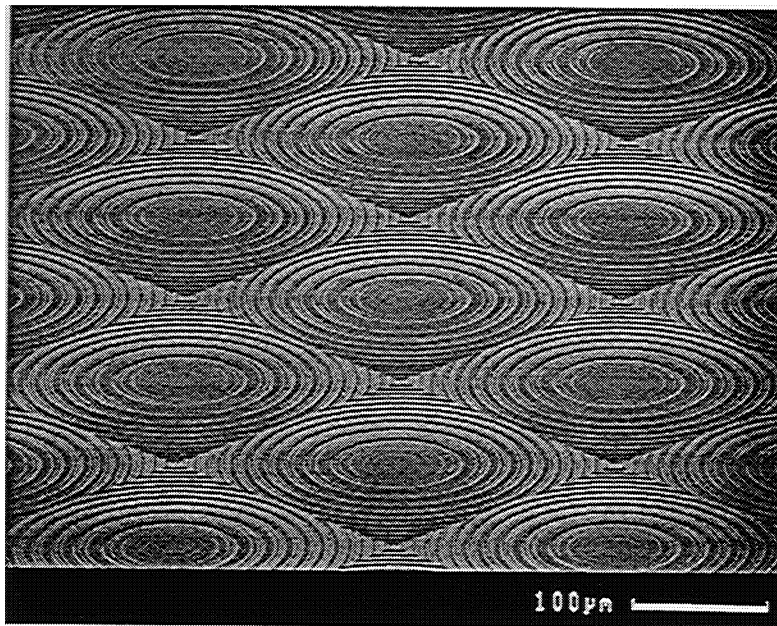


Fig. 5. Photomicrograph of a completed F/17 sapphire thin film binary optic microlens using image reversal lithography. The microlens has eight-phase levels and a speed of F/12 at the corners.

The spectral range for short wave infrared (SWIR) FPAs is from 1.5–2.5 μm and has numerous applications in medicine, security, industrial inspection, and IR astronomy, all of which will benefit from diffractive optics. High sensitivity at high operating temperature is often important in these applications. Conventional FPAs have relatively poor sensitivity and low signal-to-noise ratio at high temperatures. Integrating binary optic microlenses and hybrid FPA technologies leads to a new approach to reduce detector size, while retaining a given image resolution and optical collection area. The resultant detector volume reduction has led to a significant decrease in detector dark current and, hence, an increase in device performance.

Recent results from Rockwell⁶ show that integration of microoptics and SWIR HgCdTe can produce detectors that perform exceptionally at elevated operating temperatures. The detector configuration of this effort is shown in Fig. 6.

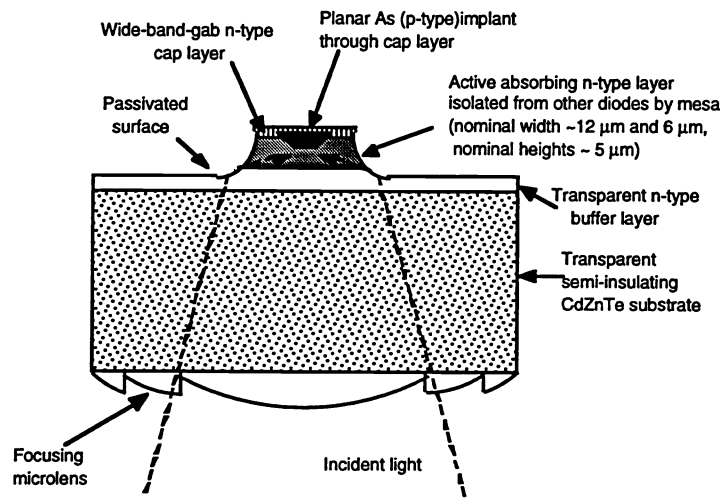


Fig. 6. Planar mesa architecture demonstrating the potential of integration of microlens with FPA

Here the incident light on the backside of the substrate is focused by a thin film binary optic to the detector forming total internal reflection; the mesa sides augment the diodes light-gathering abilities beyond the physical extent of the active layer. Note that with no buffer layer, this active area delineation is incomplete, and the effective optical area will depend on wavelength due to shorter wavelengths being more effectively absorbed by the mesa valleys which have larger area. Retaining the planar geometry on top of the mesa preserves the passivation advantage of the cap layer and as a result enhances the optical efficiency of the system.

Micro lens photolithography was done by a GCA 5X I-line stepper. The projection system requires alignment mark fiducials for mask level-to-mask level alignment on the stepper. The fiducials used by the stepper are processed first using a Karl Suss backside aligner with IR/visible light source for alignment. The Karl Suss uses an infrared light source to view circuit side fiducials through the substrate. Figure 7 shows a portion of thin film 16-phase binary optic microlens array processed by the above technique.

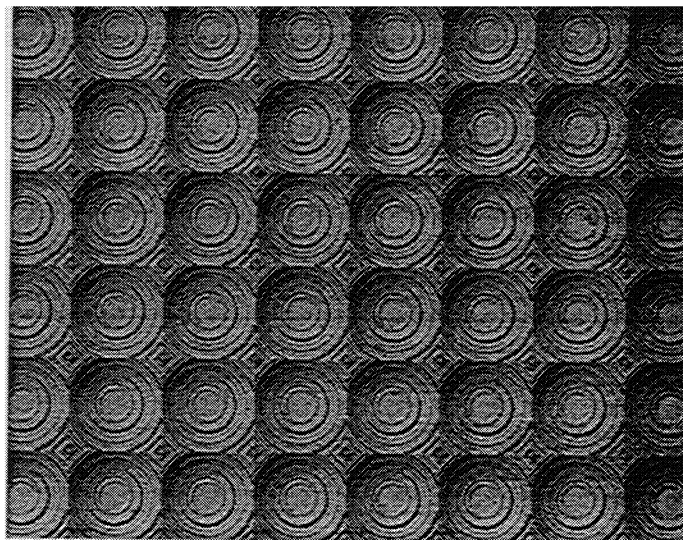


Fig. 7. A portion of 16-phase thin film microlens array processed at Rockwell.

The readout devices used in this work were simple stripline fanouts made on sapphire substrates. Hybridization was accomplished in the traditional method using cold-welded In bumps. This same technique is used for making fully multiplexed FPAs. A complete test sample consisted of a $5\text{ mm} \times 5\text{ mm}$ HgCdTe pattern which contained a 4×64 array of devices of varying types on $48\text{ }\mu\text{m}$ centers. A typical package of FPAs and microlens integration is shown in Fig. 8.

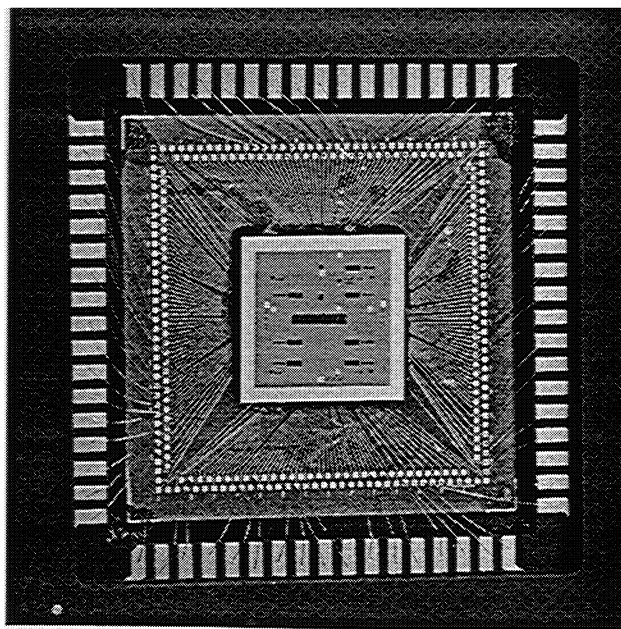


Fig. 8. A typical complete package for monolithic integration of FPAs and diffractive optics.

2.2 Refractive microlenses

Refractive microlenses may provide an attractive, low-cost alternative to diffractive microlenses. Refractive and diffractive microlenses are complementary, and in some cases refractive optics is a sole solution to optical system design. For example, in the case of a short wavelength optical system ($\lambda < 1 \mu\text{m}$) requiring high speed microlenses ($< F/4$), diffractive optics faces process limitation ($CD < 1 \mu\text{m}$).²

Refractive microlenses and microlens arrays have been fabricated by forming photoresist cylinders, then heating until the resist melts and flows, forming a refractive lens profile. Where submicron tolerances are required for coherent optical performance, process control of photoresist patterning is crucial for optimum lens quality with minimum aberration. Process issues are initial substrate cleaning, humidity control, type of the photoresist and precise control of temperature and duration of the melt process.

For applications where photoresist microlenses are incompatible with the operating environment, refractive microlenses can be generated in a suitable material by first generating photoresist microlenses, then reflowing under temperature treatment to form spherical shapes⁴ and transferring this pattern into the solid material such as silicon, GaAs, and fused silica by either reactive ion etching⁴ or ion milling.⁵ Successful microlens fabrication requires accurate control of etching and photoresist lithography processes. The fabrication issues are spatial uniformity, reproducibility and control of photoresist microlens diameter, sag and shape, reproducibility of reactive ion etch rate and selectivity, and surface roughness. Many of these issues are interrelated. The final microlens shape and dimensions depend both on the photoresist processing and reactive ion etch conditions. Thus, any variations in the photoresist lens shape may be corrected in the subsequent etch phase if the dependence of the etch behavior on process conditions (i.e., pressure, power, gas composition) is accurately known.

In the reactive ion etch pattern transfer process, the relative etch rates of the photoresist mask material and solid material can be controlled mainly by the reactive gas mixture. For fused silica microlenses, both carbon and fluorine bearing species are needed to etch silica-containing materials, while fluorine and oxygen-bearing species etch the photoresist. The gas species, pressure and temperature and RF power dependence of etch selectivity and rates need to be determined for the RIE system used in the fabrication and for the solid microlens material. The microlens arrays are usually characterized by SEM, surface profilometry and interferometric microscopy. The profilometric data are curvefit to extract the conic coefficients. For a more detailed discussion of photoresist microlens processing, conditions to achieve uniform and dimensionally accurate refractive microlens and methods of characterization, refer to references 4 and 5. In the following we will summarize some Rockwell achievements in process development, and present some design issues:

2.2.1 Process Development

Our goal was to develop a simple process to reproducibly fabricate microlens arrays that satisfy a wide range of characteristics. Modeling studies indicated that in the pattern transfer process, photoresist lens sags close (within 10%) to the desired sag in the solid material are necessary for faithful reproduction of the spherical surface. In

practice, resist microlens sag usually differs substantially from the sag of the microlens in the etched material, due to limitations of photoresist thickness imposed by the fabrication requirements. We could successfully fabricate photoresist microlenses when their aspect ratios (height to diameter ratio) were in the 3–10% range. Low aspect ratio (< 3%) resist islands did not develop into a convex surface even at the highest anneal temperatures. High aspect ratio (> 10%) islands reflowed into spherical shapes but also spread to larger diameters, severely compromising the quality of closely spaced microlenses. Within this range, formation temperature increased with decreasing aspect ratio, so that low aspect ratio levels generally required temperatures close to 200°C. Substrate type and surface preparation were critical in controlling reflowing of the photoresist.

The photoresist thickness depends on the resist viscosity, spin rate and spin time. For good uniformity, spin rate and times need to be maintained within certain limits, which restricts the range of thicknesses, hence resist lens sags, obtainable for a given type of resist. Large diameter low F# lenses require relatively thick (> 15 μm) photoresist layers. Photolithographic processing of these was difficult, generally did not result in good quality lenses, especially for closely spaced arrays; and therefore we preferred to fabricate thinner (< 15 μm) photoresist lenses and achieve thicker solid material lenses via the etch process. Because of this and the limitations on the aspect ratios discussed above, for a given lens diameter, there appears to be an optimum range of resist thicknesses that result in good quality lenses with accurate dimensions. For all of the above reasons, photoresist microlenses generally differ in sag from the sag of the solid lenses and therefore require reactive ion etching with carefully controlled etch selectivity to achieve the solid lens dimensions and surface profiles.

2.2.2 Design Issues

At Rockwell, we have designed and fabricated refractive microlenses by RIE and ion milling, in fused quartz, bulk silicon, CdTe, GaAs, InP, GaP, and by thin film deposition of Ge films on fused silica and Al₂O₃. Lens diameters ranged from 30 to 500 μm, and lens F-numbers were in the range of F/0.76–F/6. In the calculation of the lens power, the thick lens formula was used.

$$F - number = \frac{1}{2z(n(1 - z^2) - (1 - (nz)^2))} \quad (5)$$

where *n* is the refractive index, *z* = *a*/*r* with *a*, the lens radius and *r* the radius of curvature. This is exact and should be used especially for high speed microlenses (low F-numbers).

Reliable and reproducible fabrication of microlens arrays depends on accurate control of photolithographic and reactive ion etching processes. Photoresist microlenses can be reliably fabricated within a range of aspect ratios. Dimensional control of microlenses in the solid material can then be tailored by carefully controlled reactive ion etching. Both mixtures of SF₆ or O₂ with CF₃H were used to accurately control the lens sag during etching.

2.2.3 Typical refractive microlens processed at Rockwell

Rockwell has developed automated processes for both reactive ion etching and reactive ion milling to fabricate refractive microlenses with any tight performance requirement. These processes can easily control the microlens shape and conic coefficient to remove spherical aberration created by the method of photoresist reflow.

Figure 9 is SEM micrographs of a closely spaced microlens arrays. To limit the aperture to the actual lenses, the flat areas of the substrate between the microlenses were coated with a photolithographically defined layer of evaporated chrome. Figure 10 is SEM micrograph of a linear array of very fast fused silica microlens with F-number 0.86 and 80 μm diameter centers at 100 μm . Figure 11 is SEM micrograph of a InP microlens with speed of F/1 and 50 μm diameter centers at 70 μm . Figure 12 is SEM micrograph of a Ge square microlens array with speed of F/2 and 50 μm in a side centers at 60 μm .

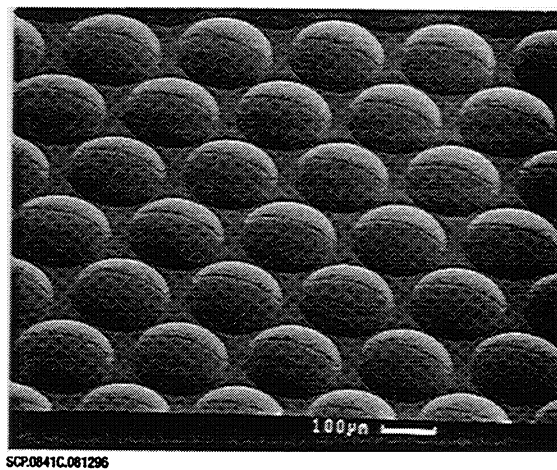


Fig. 9. SEM micrograph of a F/4.2, 200 μm diameter closely spaced microlens array fabricated in fused silica.

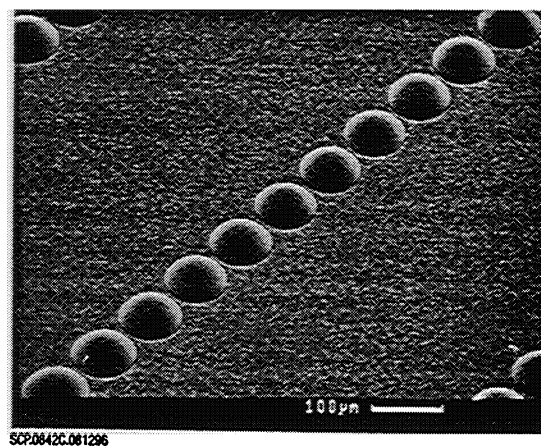


Fig. 10. SEM micrograph of a F/0.86, 80 μm diameter linear microlens array fabricated in fused silica.

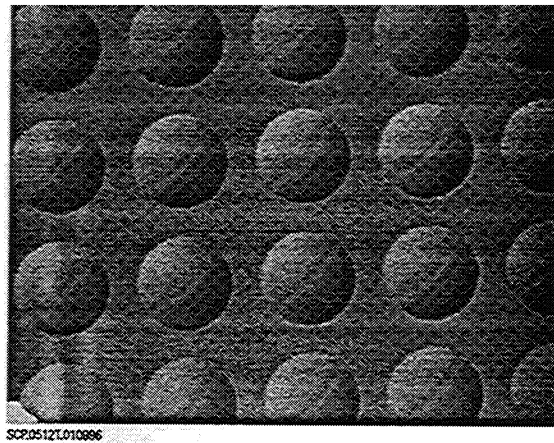


Fig. 11. SEM micrograph of a F/1, 50 μm diameter linear microlens array fabricated in InP.

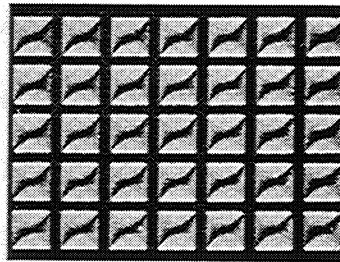


Fig. 12. SEM micrograph of a F/2, 50 μm square microlens array fabricated in Ge.

3. MICROOPTICAL MEMS: MOEM SYSTEMS

Microfabrication technology has been developed for integrated circuits and microchips during the past two decades. Remarkable progress in sculpting and micromachining added a third dimension to integrated circuits; and as a result, a 3-D microstructure could be fabricated. To make a micromachined devices dynamic, mechanical motions are combined with electronic circuits to create a new class of technology called microelectromechanical system, MEMS. Recent advances in MEMS has emerged novel subsystems, containing completely assembled motors, valves and pumps, fractions of a millimeter in size.

MEM structures can be generated by either bulk or surface micromachining processes. In bulk micromachining, structures are sculpted directly into the bulk substrate, creating 3-D features. The substrate is etched using either chemical or dry etching. Processing can occur on one or both sides of the wafer, the latter requiring back-to-front wafer alignment. In some cases the MEM structure can be formed in the substrate surface without sculpting the substrate itself. A sacrificial layer is usually used, acting as a temporary platform, to be etched away after the rest of

the MEM structure has been defined. This type of process is referred to as surface micromachining. The sacrificial layer material must be selected to provide good etch selectivity relative to the other device materials.

In the following we discuss major novelties of MEMS. We then introduce examples of the devices which require both MEMS and microoptic technologies. This class of devices (MOEM systems) will be discussed to explain on-chip optical processing:

3.1 Microsensors and microactuators

Subtechnologies under MEMS are microsensors and microactuators that recently made significant advances in device design, fabrication, materials, testing, packaging and applications. Some demanding applications of these technologies are micromotors and articulated microstructures. More ambitious applications could include actuators in a range of electromechanical systems.

A fascinating range of micromechanical sensors and actuators that could be inexpensively mass-produced using silicon micromachining and integrated circuit fabrication techniques is now envisioned. Many interesting demonstrations of MEM sensors, motors, and actuators that highlight the phenomenal possibilities for this emerging technology have been made recently. Considerable industrial attention is now being directed at MEM technology to develop applications, assisted by the impressive related capabilities that have been developed at a number of U.S. research centers.

The application of MEM technology is very much focused on the design and development of microsensor and microactuator devices. These devices have at least one dimension on the order of micrometers and are not more than several mm in the remaining dimensions. Microsensors are important elements of smart and intelligent machines and contribute much to reduce the overall system size and weight, and consequently, the cost. In recent years, MEM technology has been demonstrated to contribute extensively to reducing the size of sensors and actuators.

Microsensors/microactuators based on MEM technology have inherently the monolithic integration capability that not only reduces the device size by one order of magnitude but also tremendously improves their performance. One example of such a device is the development of a micromachined active probe designed and developed at University of Michigan for neural information processing studies. The device has 10 channels with on-chip signal processing. The channels are used for simultaneously recording the responses of the neurons. Figure 13 shows a photograph of this probe where the tip of the probe is passing through the eye of a needle.

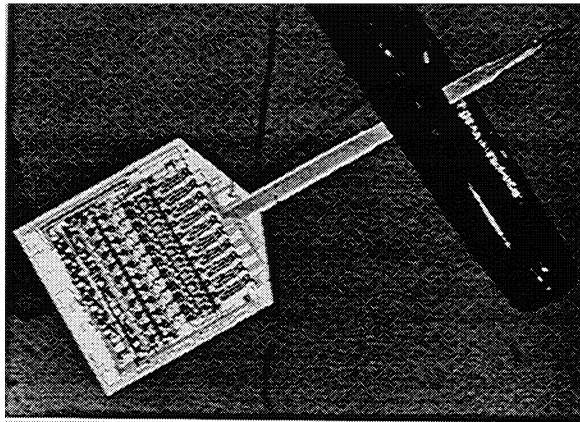


Fig. 13. 10-channel MEM probe for recording neurons developed by University of Michigan.

3.2 MOEM systems and on-chip optical processing

Both MEM and microoptic technologies have one critically important common feature: both technologies are compatible with integrated circuit (IC) processing. This feature ensures that the final device can be batch processed at low cost. The standard IC process is generally confined to the surface of the wafer (Si or GaAs), extending to within only several μm into the bulk. IC processes tailored to precisely control the etch depth and sidewalls with dimensions far inside the bulk lead to what is termed a three-dimensional integrated circuit or, more commonly, micromachined circuits. Micromachining is also a common process requirement for both microoptic and MEM technologies. The overlapping of the three major fields—electronics, mechanics, and optics or merging microoptics and micromechanics (MOEM systems)—is required to be succeeded in integration of optical processing. We will now discuss devices that represent MOEM systems and that have the potential of being candidates for on-chip optical processing.

In the past several years, researchers proposed and demonstrated many applications of MOEM systems. Most of these demonstrations are based on miniaturized systems with microoptics and micromechanics, where fabrication of all the optical and MEM components on a single chip was not necessary.

The recent development at UCLA of surface micromachined microhinge and free space integrated optics¹⁰⁻¹⁴ resulted in a microoptical bench that has attracted much attention for optical processing on-chip. Free-space integrated optics offers many advantages over the guided-wave approach, such as high spatial bandwidth (diffraction limited), non-interfering optical routing, three-dimensional optical interconnection, and optical signal processing capability (e.g., Fourier optics). However, it is more difficult to integrate free-space optics on a single substrate since most monolithically fabricated free-space optical elements lie on the surface of the substrate.

Micromachining of silicon substrate has been applied to integrated optics and the realization of miniature optical bench. Also, surface micromachined hinges and spring-latches¹⁰ have been used to achieve monolithic fabrication of

three-dimensional micro-optics.¹³ This technology opens a new area for integrated optics in free space. Using this new technique, three-dimensional micro-optical components can be fabricated integrally on a single Si chip. The Si substrate serves as a micro-optical bench on which microlenses, mirrors, gratings and other optical components are prealigned in the mask layout stage using computer-aided design and then constructed by microfabrication. Additional fine adjustment can be achieved by the on-chip micro-actuators and micropositioners such as rotational and translational stages. With hybrid integration of active optical devices, a complete optical system can be constructed, as illustrated in Fig. 14.

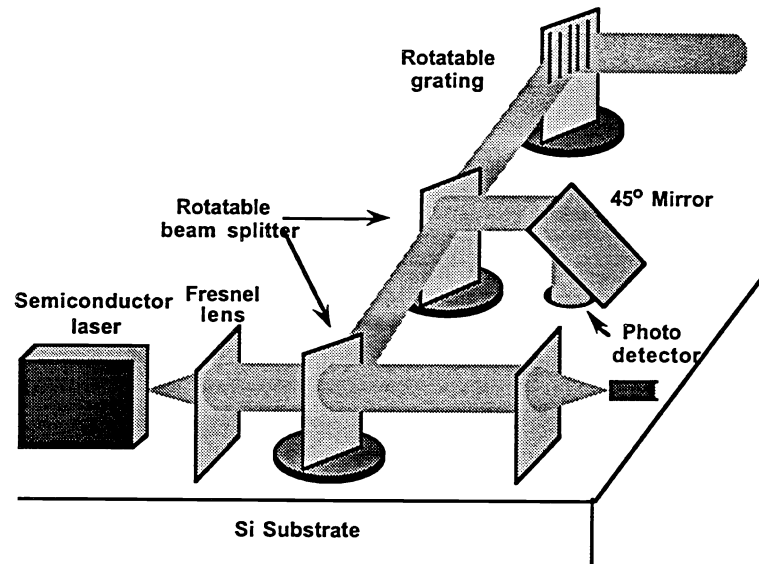


Fig. 14. The schematic diagram illustrating the micromachined free-space microoptical system on a single Si chip.

The three-dimensional microoptical system is constructed on a Si substrate by the surface micromachining technique. In the following, we discuss some of the major components of a typical optical train required for on-chip optical processing.

2.2.1 Microbase, micromount, and microhinge design

The micro-optics plates used for mirror, beam splitter, microlens array, grating, and collimator are processed by surface micromachining, and they are released from the substrate by selectively removing the sacrificial material (deposited SiO₂) using hydrofluoric acid after fabrication. After the release etching, the poly-plates with microoptics patterns are free to rotate around hinge pins (Fig. 15).

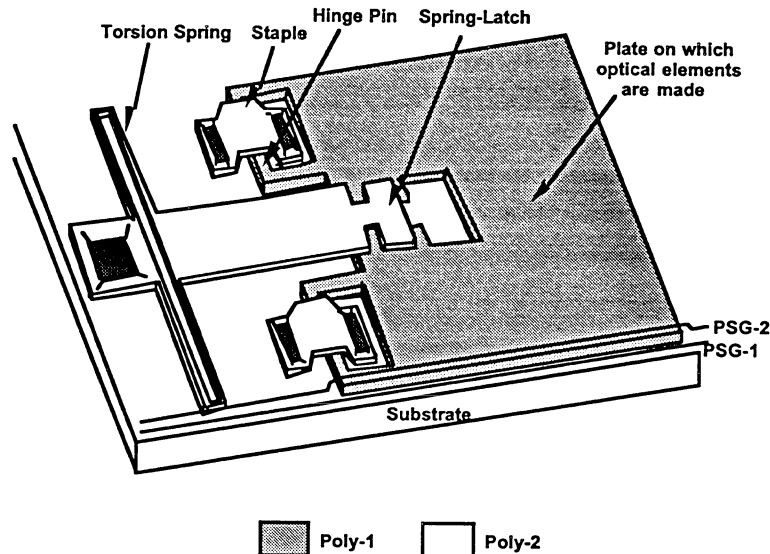


Fig. 15. The schematic structure of MEM microoptical elements before assembly.

When the plate is lifted up, the top portion of the spring-latch slides into the slot on the plate, and snaps into a narrower part of the slot, thus preventing further motion of the plates. The torsion-spring connecting the spring-latch to the substrate creates the spring force, which tends to force the spring-latch back to the substrate, therefore locking the plate in its place. The length of the spring latch defines the angle between the plate and the substrate. After the three-dimensional micro-optical element is assembled, a layer of gold is coated on the lifted poly surfaces. In binary-amplitude Fresnel zone plates or micro-mirrors, a thick layer of gold is needed to completely block the light passing through the dark zones or to make a perfectly reflecting mirror. On the other hand, thinner gold is desired for partially transmitting mirrors or beam splitters.

2.2.2 Fresnel microlenses

Figure 16 shows the SEM photograph of a three-dimensional Fresnel micro lens after assembly. The diameter of this lens is $280\ \mu\text{m}$, with a designed optical axis of $254\ \mu\text{m}$ for passive integration of an edge-emitting semiconductor laser. Because of the height of the lens plate, the angles between the lens plates and the substrate have some variations even though they are coarsely defined by the spring latches. Such variations are not tolerable in large optical systems. Therefore, a new set of "lens-mount" is designed to precisely define the angles of the three-dimensional microoptical elements. The lens mount consists of two folded polysilicon plates which are fabricated integrally with the microlens. The lens mount has a V-shaped opening at the top to guide the lens plate into a $2\text{-}\mu\text{m}$ -wide groove in the center. It can be made as tall as the lens itself, therefore, the angle defined by the lens mount are much more precise. The lens mount also greatly improves the mechanical strength and stability of the microoptical elements.

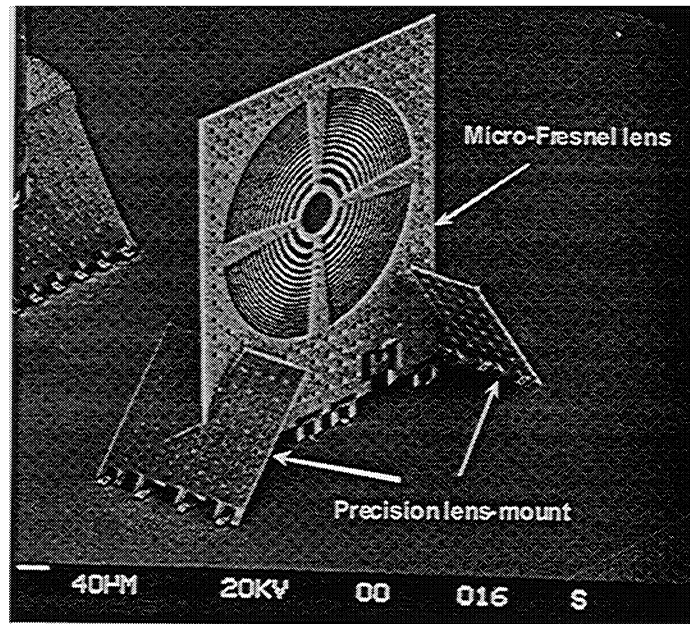


Fig. 16. SEM photograph of a Fresnel microlens with precision lens-mount.

The optical performance of the three-dimensional Fresnel microlens has been tested by collimating a divergence beam emitted from a single mode fiber at $\lambda = 1.3 \mu\text{m}$. The intensity FWHM divergence angle is reduced from 5.0° to 0.33° by the lens. The collimated beam profile fits the Gaussian shape (95% fit) very well.

2.2.3 Translation stage

One unique feature of implementing micro-optical bench using surface micromachining is that micropositioners and microactuators can be monolithically integrated in the same fabrication processes for different type of optical translators. This allows the alignment of the optical systems to be fine adjusted, in addition to the coarse alignment done at the design stage using CAD layout tools. Using similar structures as the micromotors, rotational stages and linear micropositioners can be realized. UCLA researchers have successfully integrated the three-dimensional micro-optical elements with rotational stages using this process. Figure 17 shows the SEM photograph of a rotatable mirror. The rotatable plate is fabricated on the first polysilicon layer, and the axis and hub are defined on the second polysilicon layer. The indicator on the lower part of the picture, originally pointing at the 0° tick, has been rotated counterclockwise by 20° after the mirror is assembled, as shown on the picture. A diffraction grating integrated with the rotational stage is successfully demonstrated using the same technology, as shown in Fig. 17.

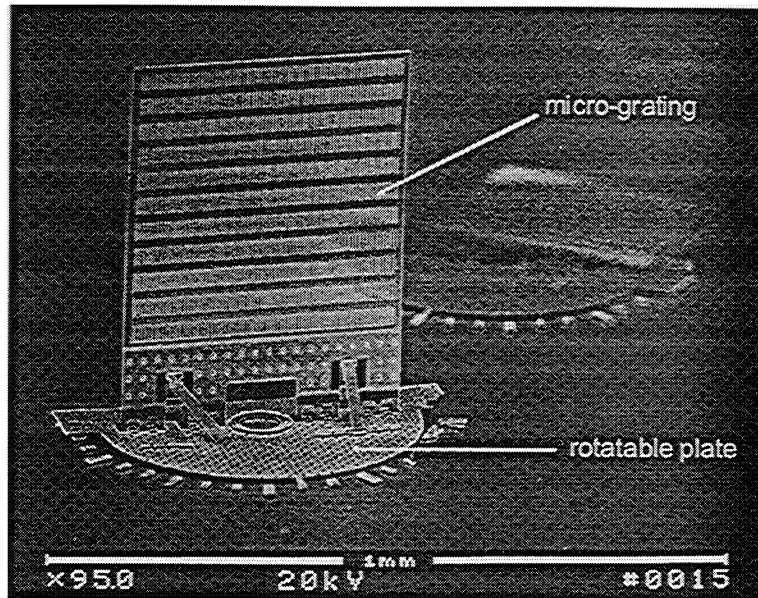


Fig. 17. The diffraction grating integrated with a rotational stage.

4. POTENTIAL APPLICATIONS

In this section we review recent developments and achievements in both microoptics and MEM and introduce several attractive MOEM devices that have recently been proposed and are being developed at different laboratories. These optical subsystems have capabilities that enable complete integration on a single chip.

4.1 3-D Tunable Fabry-Perot

Tunable Fabry-Perot (FP) etalons are very useful for wavelength-division-multiplexed (WDM) optical communications, optical sensing, and spectral analysis applications. There has been a great deal of interest to apply the micromachining technology to realize compact tunable FP etalons, since most FP etalons are tuned mechanically. Many micromachined FP etalons have been demonstrated, including a vertical single-crystal bulk-micromachined Si resonator created by deep dry etching,¹⁵ a surface-micromachined membrane on Si,¹⁶ and epitaxially grown GaAs/AlGaAs cantilevers.¹⁷ However, most of the surface-micromachined filters lie on the surface of the substrate, and cannot be integrated with other microoptical elements on the same chip. Here, we demonstrate a novel three-dimensional tunable filter implemented on the surface-micromachined free-space microoptical bench (FS-MOB).^{18,19} It can be readily integrated with other microoptical elements (e.g., collimating and focusing lenses, or cascaded tunable filters for WDM demultiplexers) or fiber alignment V-grooves. Both parallel-plate FP etalons and solid FP etalons have been realized by the FS-MOB technology.

The schematic drawing and the SEM micrograph of a solid FP etalon are shown in Fig. 18(a) and 18(b), respectively. The etalon is fabricated by the three-polysilicon layer surface-micromachining technique. The microhinge allows the etalon to be folded into three-dimensional structures after fabrication. The etalon is integrated with a rotation stage for angle tuning of the transmission wavelength. Both surfaces of the polysilicon etalon plate are coated by three pairs of quarter-wavelength SiO_2/Si dielectric layers to increase their reflectivity. The transmission wavelength versus the rotation angle of the etalon is shown in Fig. 19 (a). A very broad tuning range of 58.5 nm is obtained when the etalon is rotated by 70° . The experimental data agrees very well with the theoretical analysis using transmission matrix approach. Figure 19 (b) shows the transmission spectrum of the etalon at 50° rotation. The finesse of the etalon is measured to be 11, currently limited by the scattering loss due to the granular surface of the polysilicon plate. The finesse could be improved by using parallel plate FP etalons and smoothing the surface of the polysilicon plates using chemical mechanical polishing.

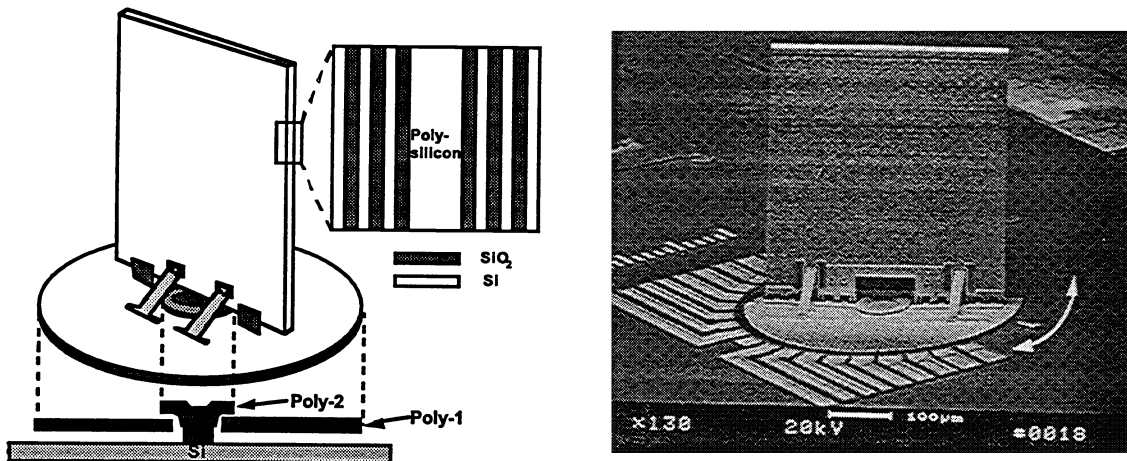


Fig. 18. The schematic and SEM of the tunable solid Fabry-Perot etalon.

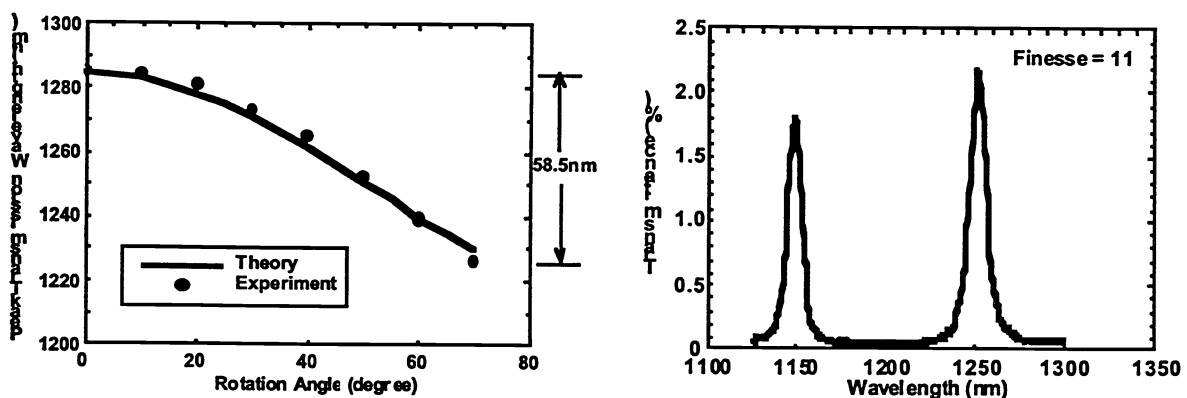


Fig. 19. The wavelength tuning range and the transmission spectrum of the tunable filter.

4.2 FDDI Optical Bypass Switch

The surface-micromachining technique has also been used to demonstrate a single-chip 2×2 optical bypass switch for FDDI (Fiber Data Distribution Interface) local area networks. The bypass switch is used in FDDI fiber ring networks to bypass failed computer nodes and enhance the network reliability (Fig. 20). It is also useful for reconfigurable optical fiber networks. Free-space opto-mechanical switches offer several advantages over conventional waveguide switches. Very low insertion loss and small crosstalk can be achieved by the free-space approach. In addition, no standby power is required after the switch is reconfigured. Si bulk-micromachining and wafer bonding techniques have been used to implement free-space opto-mechanical switches.²⁰ However, monolithic integration is difficult and substantial assembly is still required. Here, we propose to use the surface-micromachining technology to monolithically integrate the free-space microoptical switch with microactuators and fiber optic alignment guides²¹. They can be made compact and light weight, and are potentially integrable with the optical sources/detectors and controlling electronics. Moreover, since the switch is made by photolithographic process, the optical elements can be prealigned during the layout of the photomasks. The assembly and packaging cost can also be reduced.

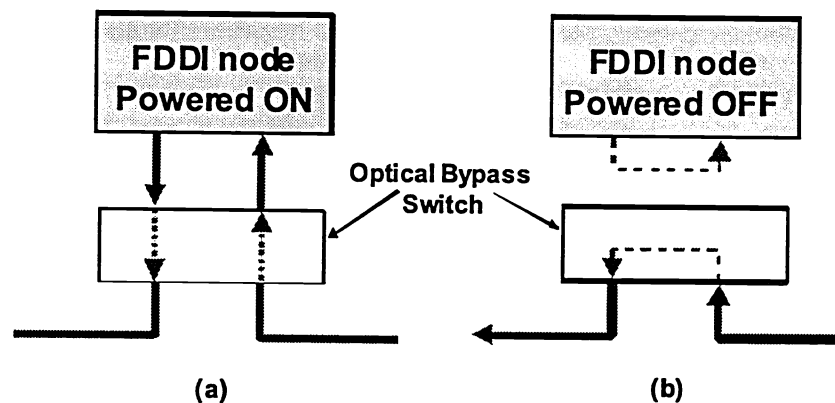


Fig. 20. Schematic diagrams of (a) normal operation and (b) bypass state of the FDDI optical bypass switch.

The switch consists of a three-dimensional movable mirror and four optical fiber guiding rails, as shown in Fig. 21. Four multimode fibers are arranged in a "cross" configuration, with a movable micromirror placed in the center. The switch operates in two states: CROSS and BAR states. When the mirror/sliding-plate is moved away from the fibers (the center), the fibers along the same diagonal directions are allowed to communicate with each other. This is defined as CROSS state. In the BAR state, the mirror/sliding-plate is slid into the center and the light signal is reflected to the orthogonal fiber. Since no bulk optical lenses are used, the spacing between fiber tips is minimized to reduce optical diffraction loss. Alternatively, integrated out-of-plane refractive microlenses can be used to further reduce the diffraction loss. The movable micromirror consists of a gold-coated out-of-plane polysilicon plate integrated on a sliding plate. The fabrication processes have been described earlier. Figure 22 shows the SEM micrograph of the switch. The top-view photographs of the switch in CROSS and BAR states are shown in Fig. 23 (a) and (b), respectively.

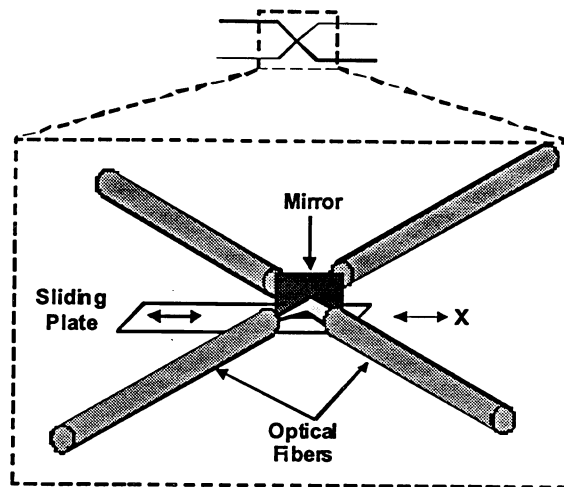


Fig. 21. Schematic diagram of the surface-micromachined FDDI optical bypass switch.

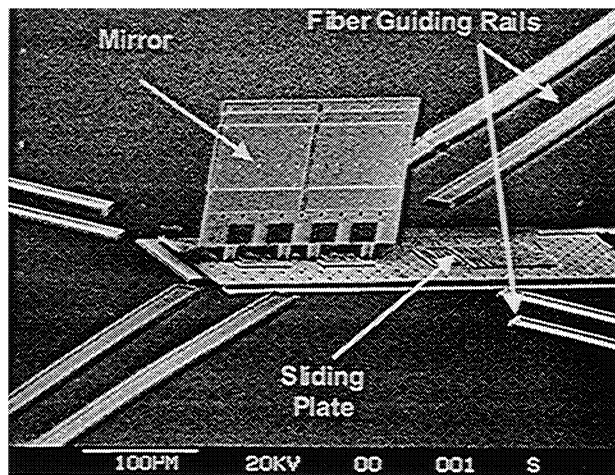


Fig. 22. The SEM of the three-dimensional mirror sitting on a sliding plate.

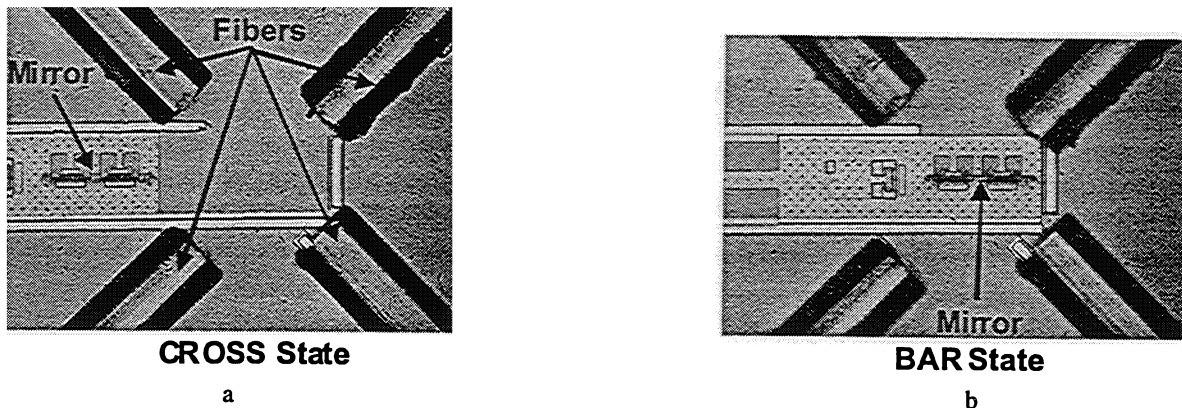


Fig. 23. The top-view photographs of the switch in (a) CROSS state and (b) BAR state.

The optical performance of the optical switch is characterized by attaching multimode fibers to the guiding rails of the optical fibers. The insertion loss of the switch for both operating states has been measured with a LED source operating at $1.3 \mu\text{m}$ wavelength. The total insertion loss of the switch has been measured to be 2.8 dB for the CROSS state and 3.1 dB for the BAR state. From these two measurements, the reflectivity of the mirror is estimated to be 93%. The crosstalk between two states is measured to be 26.1 dB. In principle, the theoretical coupling loss between multimode fibers was estimated to be 1 dB for fiber-to-fiber spacing of $125 \mu\text{m}$, and 0.45 dB for fiber-to-fiber spacing of $50 \mu\text{m}$ ²². The excess loss measured here includes the Fresnel loss of the fiber (~ 0.34 dB), and possible misalignment of the fibers. Recently, the insertion losses have been reduced to 1.4 dB and 1.9 dB, respectively, with an improved design. The diffraction loss is reduced by using lensed fibers for both input and output fibers. Micromachined integrable lenses, antireflection coated fibers, and smoother mirror (by chemical mechanical polishing) can be used to further improve the performance of the switch.

4.3 MEM Corner Cube Reflector

Micromachined corner cube reflectors (CCRs) fabricated at UCLA have demonstrated the concept of transmitting data digitally by modulating reflected light intensity. Corner cube reflectors ranging in size from 100 to $200 \mu\text{m}$ have been built using hinged polysilicon plates. The reflectivity of polysilicon has been measured to be 24% and the total reflected power from the corner cube has been measured to be between 1 to 2% of the incident power. Orthogonality between plates is within roughly 8 mrad. Reflection from individual polysilicon plates has been modulated using electrostatic actuation with an applied voltage as low as 8 V.

Corner cube reflectors have been used in optical systems mainly because, unlike other optical components, they are not critically sensitive to misalignment. A beam of light that hits a defined active area in the concave side of a three-sided orthogonal corner will be reflected back along the axis of arrival to the source. Rays which hit outside this active area do not exit parallel to themselves and therefore do not contribute to the reflected beam. Reflectors of this type are called CCR. If the orthogonality of the corner cube is disturbed, then the impinging light will not be reflected back to the source. Hence, it is possible to modulate the intensity of the reflected light by small motions of

one or more sides of the corner cube. This light modulation can be used to transmit data from the corner cube to the light source with very little power used by the corner cube.

A schematic diagram of the top view of a corner cube reflector is shown in Fig. 24. The device is designed using MUMPS process. Each corner cube is made of four 100-200 μm square polysilicon plates rotated out of the surface of the wafer using microfabricated polysilicon hinges as described in Ref. 10, and a long plate suspended by 100-200 μm long thin beams on either side. Two of the rotated plates form the right-angled corner while the remaining two plates serve as supports and orthogonal aligners for setting up the device as a CCR. The long suspended plate also functions as an integral torsional deflection actuator. This plate is actuated electrostatically to deflect the light, thus modulating the reflected intensity. Beneath this plate are two electrodes. One is the landing electrode at the end of the plate and the other is the forcing electrode. Figure 25 shows a complete processed corner cube device set up for CCR measurements.

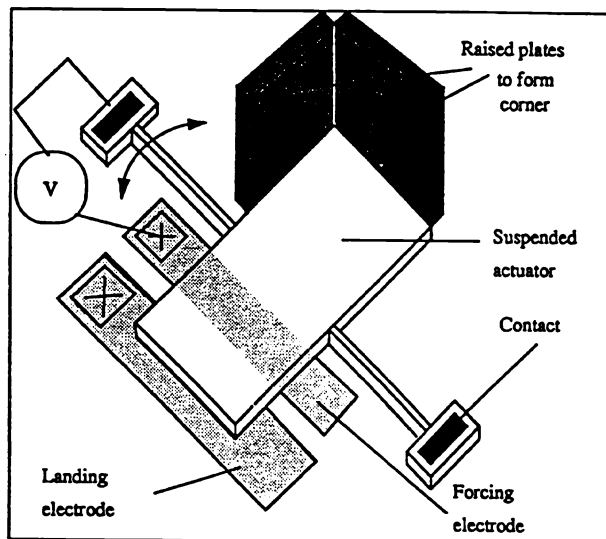


Fig. 24. Schematic diagram of the top view of the corner cube reflector.

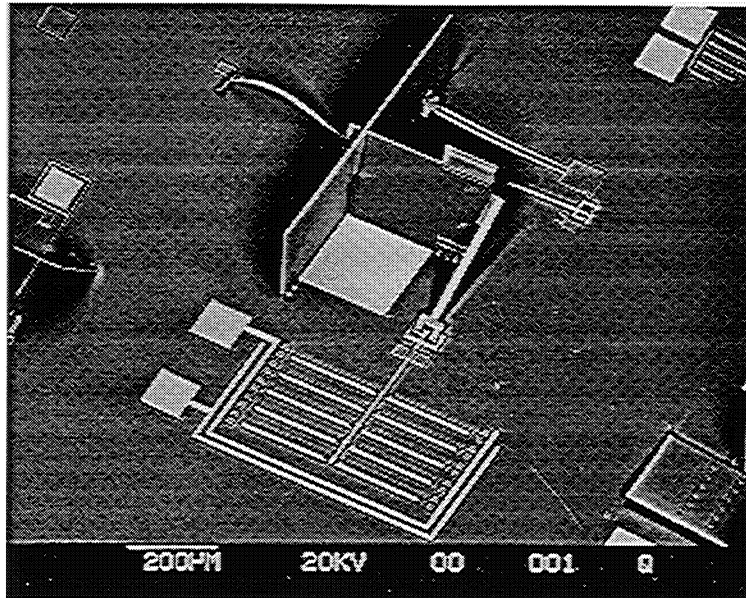


Fig. 25. A corner cube device fabricated using MUMPS process.

To use the corner cube concept as a communication link, the system consists of a number of remote units and one or more base stations. Each remote unit contains a sensor, electronics, a corner cube, a photodiode and a power source. The sensor can be customized for each application. The base station contains a laser source and a photosensor to detect the signal reflected from the corner cube. When the photodiode detects a coded signal from an interrogating laser, the electronics system amplifies, conditions and digitizes the output from the sensor and feeds the data into a shift register which starts to output the signal one bit at a time in the form of a voltage that actuates the CCR. A photodetector, placed in close proximity to the source, will then detect the data transmitted and demodulate it to give the inquirer a digital readout of the sensor output. In a more advanced system, a control system can be integrated so that the base station may send instructions to the remote sensor.

A corner cube sensor as described here has several advantages. Because of its miniature size, the actuation process requires very little power. Thus, the remote unit needs only to have a low power supply residing within it. A CMOS electronics system can be integrated on-chip. This capability, together with the low power consumption, makes the remote unit completely autonomous. In the communication process, the detector does not have to hunt for the reflected signals. As long as it is placed very close to the source, it is guaranteed to receive the transmission. This provides an intrinsically secure communication channel since competing receivers will not be able to tap into the communication process.

4.4 Digital video using DMDs

Digital video technology is becoming increasingly important to the networked society and opening a new technology direction for low-cost projection displays. The natural interface to digital video is a digital display. A digital display

accepts electrical bits at its input and converts them into optical bits at the output. The digital-to-analog processing function is performed in the mind of the observer. Texas Instruments has developed such a display with its recent market introduction of the Digital Light Processing™ (DLP™) projection display. DLP technology is based on the Digital Micromirror Device™ (DMD), a MEMS array of semiconductor-based digital light switches. The DMD switching array precisely controls a light source for projection display and digital printing applications. Here we present an overview of DLP technology along with the architecture, projection operation and new advances of the DMD development.²⁴⁻²⁹

The growth of the global networked society is being driven by the degree to which a common “digital language” is spoken. Digital video technology has become increasingly important to this networked society because of three digital characteristics: (1) the ease of manipulation of bits for purposes of reducing bandwidth (compression) and for mixing audio, text, graphics, and video (multimedia); (2) the fidelity of digital transmission {e.g., direct broadcast satellite (DBS)}, digital storage and playback {e.g., digital versatile disc (DVD)}; and (3) the possibility of limitless reproduction without degradation.

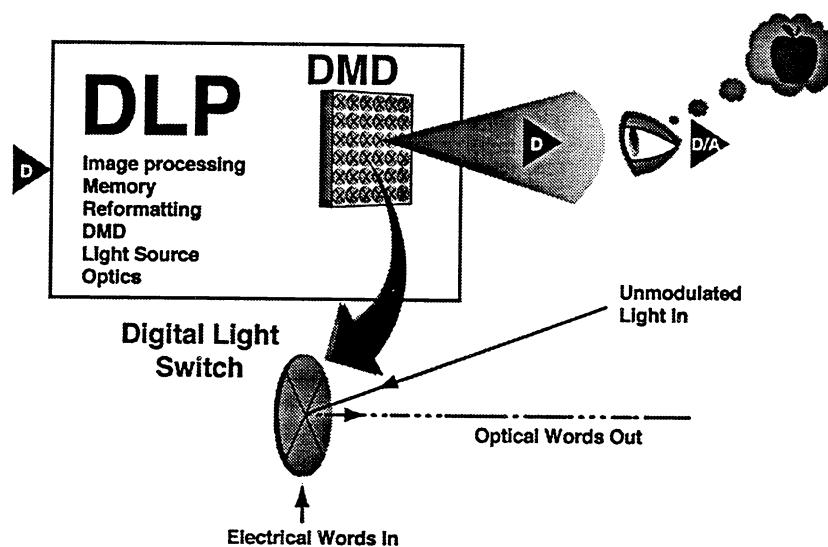


Fig. 26. Digital light processing system

Figure 26 shows such a digital display based on the Digital Light Processing production display. DLP is based on a MEMS device known as the Digital Micromirror Device. Invented in 1987 at Texas Instruments, the DMD is an array of fast, reflective digital light switches. It can be combined with image processing, memory, a light source, and optics to form a DLP system capable of projecting large, bright, seamless, high-contrast color images with better color fidelity and consistency than current displays. DLP systems can also be configured to project images for the production of continuous tone, near photographic quality printing. Numerous publications and presentations have been made on all aspects of DLP and DMD technology, including DLP projection displays.

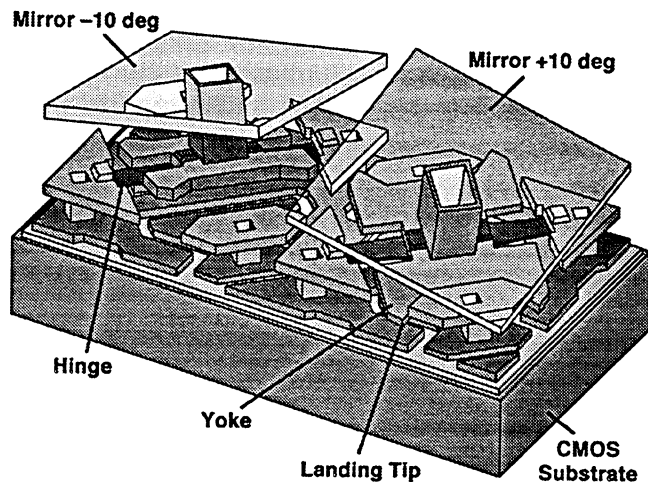


Fig. 27. Two DMD pixel where mirror is shown transparent and rotated

The DMD light switch (Fig. 27) is a MEMS structure that is fabricated by CMOS-like processes over a CMOS memory. Each light switch has an aluminum mirror, $16\ \mu\text{m}$ square, that can reflect light in one of two directions depending on the state of the underlying memory cell. With the memory cell in the (1) state, the mirror switches to +10 degrees. With the memory cell in the (0) state, the mirror switches to -10 degrees. By combining the DMD with a suitable light source and projection optics (Fig. 28), the mirror reflects incident light either into or out of the pupil of the projection lens. Thus, the (1) state of the mirror appears bright and the (0) state of the mirror appears dark, and the gray scale is achieved by binary pulsewidth modulation of the incident light. Color is achieved by using color filters, either stationary or rotating, in combination with one, two, or three DMD chips.

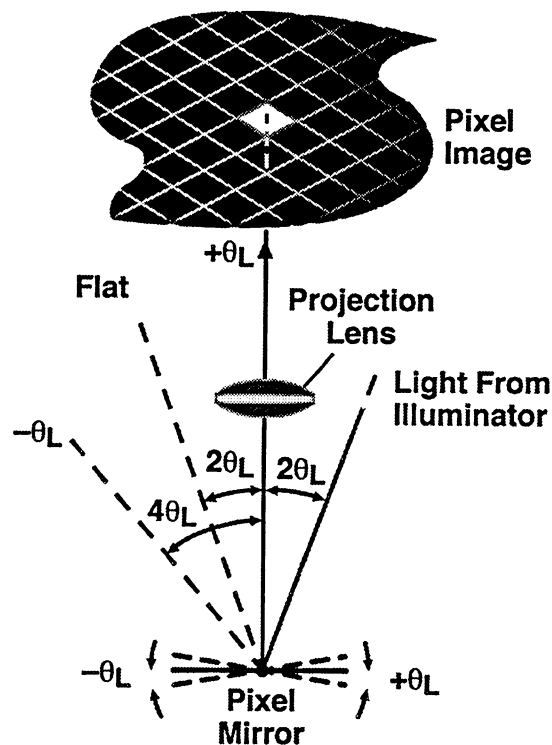


Fig. 28. Optical switching principle of DMD

This mirror structure has been migrated to the 848×600 (SVGA) pixel DMD, and contrast ratios from both front and rear projection systems based on such mirrors routinely exceed 100:1. We believe this performance will enable the creation of commercially viable systems. With a between-mirrors gap of 1.0 micron, current DMDs with this mirror structure have an aperture ratio of 89%. The technology is expected to achieve a 0.8 micron between-mirrors gap that will result in an ultimate aperture ratio of 91%. Higher contrast ratios can be achieved by limiting the aperture of the projection lens, thus discriminating preferentially in favor of reflected rather than diffracted light, but system throughput is reduced. Such trade-offs may be justified in nondisplay imaging applications where wider dynamic ranges are required. Contrast ratios exceeding 400:1 have been observed in such systems.

The DMD pixel is a monolithically integrated MEMS superstructure cell fabricated over a CMOS SRAM cell (Fig. 29). An organic sacrificial layer is plasma-etched to produce air gaps between the metal layers of the superstructure. The air gaps free the structure to rotate about two compliant torsion hinges. The mirror is rigidly connected to an underlying yoke. The yoke in turn is connected by two thin, mechanically compliant torsion hinges to support posts that are attached to the underlying substrate.

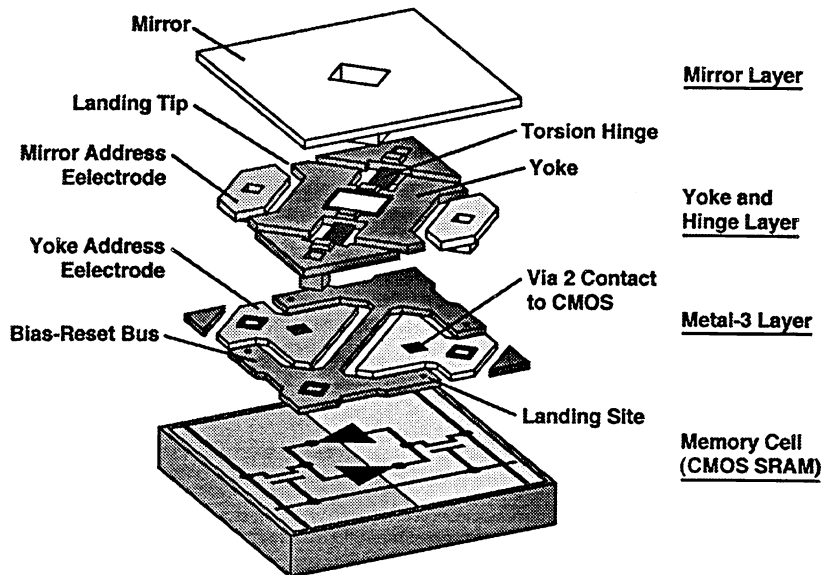


Fig. 29. DMD pixel exploded view

Electrostatic fields are developed between the underlying memory cell and the yoke and mirror, creating an electrostatic torque. This torque works against the restoring torque of the hinges to produce mirror rotation in the positive or negative direction. The mirror and yoke rotate until the yoke comes to rest (or lands) against mechanical stops that are at the same potential as the yoke. Because geometry determines the rotation angle, as opposed to a balance of electrostatic torques as in earlier TI devices, the rotation angle is precisely determined. The address electrodes for the mirror and the yoke are connected to the complementary sides of the underlying SRAM cell. The yoke and mirror are connected to a bias bus fabricated at the Metal-3 layer. The bias bus interconnects the yoke and mirrors of each pixel to a bond pad at the chip perimeter. An off-chip driver supplies the bias waveform necessary for proper digital operation.

The recent reports from Texas Instruments indicate that a higher-resolution DMD has been achieved with the fabrication of a 1280×1024 (SXGA) mirror resolution. There are several challenges to the fabrication of such high-resolution DMDs. These devices have potential use for commercial display applications.

4.5 2-D optical scanner

We present here a 2-D optical scanner developed at Rockwell to modulate the direction of a laser signal. Applications include beam steering components of laser radar and optical communication systems. Conventional methods that use bulk optical components can result in systems that are too heavy and not desirable for applications that require rapid optical beam steering, low rotational and translational inertia and small component displacements. Microoptic beam

steering systems fulfill these requirements, achieving a field of view of more than 10° , with only a fraction of a millimeter of component translation.

The microlens beam steering device design presented here is based on dithering two complementary (positive and negative) microlens arrays. When the two microlenses are translated relative to each other in the plane parallel to their surfaces, a light beam can be scanned with a two-dimensional array of spots. We have demonstrated a miniaturized module consisting of a pair of 6 mm-aperture binary optic microlens arrays designed for HeNe laser operation. The system can scan the laser beam at rates of 200 Hz or greater. The microlens arrays are optically flat with surface relief on the order of one optical wavelength, permitting separation distances of several microns. Individual lenslet sizes can be in the range of 100–200 μm , resulting in maximum translation of similar magnitude. Reducing both the inertia and the travel of the lens system makes the device suitable for agile beam steering.

The microlens arrays were fabricated out of fused quartz using photoresist masking and reactive ion etching. The microlens chips were sawed from a 0.4 mm thick wafer in squares 10 mm on a side. Each array is driven by a piezoelectric actuator, the two arrays being driven in orthogonal directions. The ultimate module field of view of 10° is achieved by translating the array by one-half of a lenslet diameter, which is $\pm 100 \mu\text{m}$.

Optical testing was performed on the beam steering module. The center lobe contains most of the beam energy. The rest of the energy is distributed among the neighboring addressable points. A computerized test bed with a customized D/A converter board was used to generate drive signals for the scan actuators. Programmable patterns of test signals were output to the piezoelectric transducers to control the beam angle in two dimensions. For more details of scanner operation, refer to reference 30.

The characteristics of the 2-D scanner are shown in Fig. 30. Figure 30(a) is a photograph of the scanner output when the beam is stationary. Figure 30(b) is a plot of point spread function measurements, which agree with visual observation. Figure 30(c) is the result of a linear scan by removing the x-direction signal and scanning only in the y-direction.

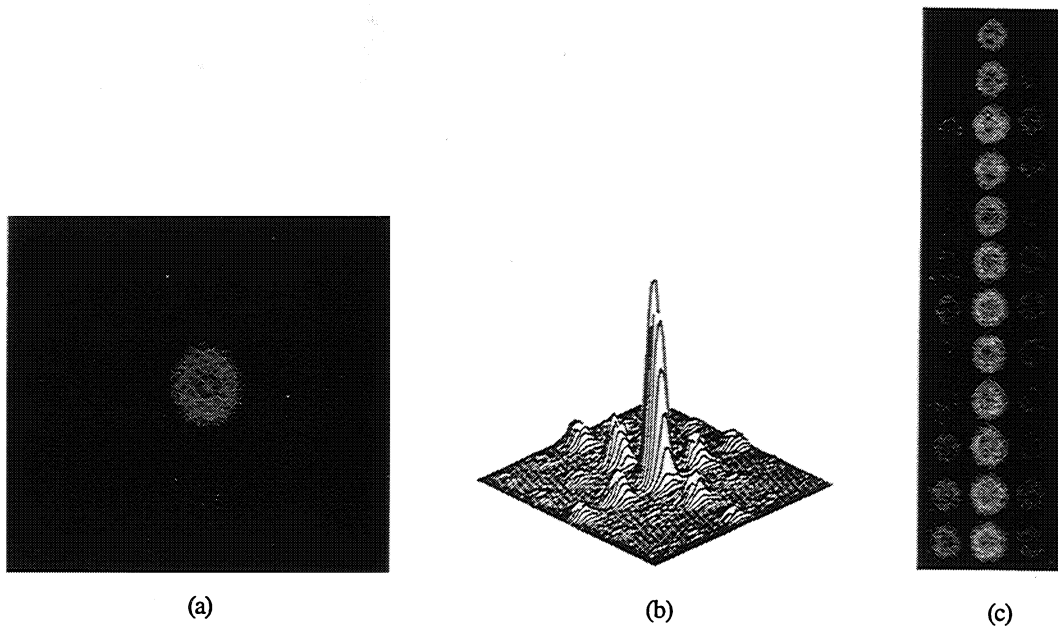


Fig. 30 Characteristic of 2-D Microlens Scanner developed by Rockwell.

The resulting patterns showed, as predicted, very uniform and well-aligned spots where the majority of the energy is diffracted into a single peak, with lesser amounts into neighboring peaks. The scanner was demonstrated up to a rate of 300 Hz. Operation at higher than 1 KHz is possible with appropriate damping of mechanical resonances. A random point steering was tested experimentally by programming our computerized test bed. The pointing was randomly designed inside an array of 13×13 addressable points. Switching between two points was less than 5 ms.

Rockwell has developed a miniaturized package for microlens scanner. MEM actuators are planned to be used to reduce the size of this laser scanner package possibly by two orders of magnitude. Using this approach, we expect to reduce the size of the optical scanner to less than one cubic centimeter.

5. CONCLUSIONS

Microoptics technology including both diffractive and refractive microlenses has advanced significantly over the past several years. The use of similar micromachine processes for microoptics and micromechanics offers the promise for further technology integration, the development of micro-opto-electro-mechanical (MOEM) technology. This enables the incorporation of optical functions into microdevices, resulting in another whole new field for sensors and other microdevices to be candidates for on-chip optical processing. Examples include 3-D tunable Fabry-Perot, FDDI switch, corner cube reflector, digital video, DMDs, and 2-D laser scanner. These technologies are expected to rapidly gain in maturity, as they all rely on the identical batch processing. We have presented here a few recent developments in this emerging field and have described examples of devices that are being developed. Further significant rapid advances can be expected for on-chip optical processing as researchers recognize the full range of functionality that can be realized using this exciting new technology.

6. ACKNOWLEDGMENTS

The authors gratefully acknowledge Dr. Larry Hornbeck at Texas Instruments, and Dr. Haluk Sankur at Rockwell Science Center for their contributions to this paper. This work was supported by Rockwell IR&D and DARPA. Section 4.4 (Digital video using DMDs) has been adapted with permission of the author [ref 24].

7. REFERENCES

1. M.E. Motamedi, W.H. Southwell, R.J. Anderson, W.J. Gunning, M. Holz, "High Speed Binary Microlens in GaAs", *Proceedings, SPIE*, Vol. 1544, pp. 33–44, July 1991.
2. M.E. Motamedi, M.P. Griswold, R.E. Knowlden, "Silicon Microlenses for Enhanced Optical Coupling to Silicon Focal Planes", *Proceedings of SPIE*, Vol. 1544, pp. 22–32, July 1991.
3. M.E. Motamedi, B. Anderson, R. De La Rosa, W.J. Gunning, R.L. Hall, M. Khoshnevisan, "Binary Optics Thin Film Microlens Array", *Proceedings, SPIE*, Vol. 1544, pp. 22–32, July 1992.
4. H.O. Sankur, R.L. Hall, M.E. Motamedi, W.J. Gunning, W.E. Tennant, "Fabrication of IR microlens arrays by reactive ion milling," *SPIE Proceeding of Miniature and Micro-optics and Micromechanics*, Vol. 2687, pp. 150-155, 1996.
5. H.O. Sankur, M.E. Motamedi, R. Hall, W. Gunning, M. Khoshnevisan, "Fabrication of refractive microlens arrays." *SPIE Proceeding of Miniature and Micro-optics and Micromechanics*, Vol. 2383, pp. 179-183, 1995.
6. M.E. Motamedi, W.E. Tennant, R. Melendes, N.S. Gluck, S. Park, J.M. Arias, J. Bajaj, J.G. Pasko, W.V. McLevige, M. Zandian, R.B. Hall, K.G. Steckbauer, P. D. Richardson, "FPAs and thin film binary optic microlens integration," *SPIE Proceeding of Miniature and Micro-optics and Micromechanics*, Vol. 2687, pp. 70-77, 1996. (invited paper)
7. M.E. Motamedi, W.H. Southwell, H.O. Sankur, R. Melendes, M. Khoshnevisan, F. Durville, X. Wang, C. Liu, R. Rediker, J. Leger, "Optical transformer and collimator for efficient fiber coupling," to be published in proceedings of SPIE conference on "Miniaturized system with microoptics and micromechanics," in San Jose, CA, on February 8-14, 1997. (invited paper)
8. M.E. Motamedi, "Merging Microoptics with Micromechanics: Micro-opto-electro-Mechanical (MOEM) Devices", *Proceedings, SPIE*, Vol. CR49, pp. 302–328, July 1993 (invited paper).

9. M.E. Motamedi, "Micro-opto-electro-mechanical systems," *Optical Engineering*, Vol. 33, No. 11, pp. 3505- 3517, Nov. 1994. (invited paper).
10. K.S.J. Pister, M.W. Judy, S.R. Burgett, and R.S. Fearing "Microfabricated hinges", *Sensors and Actuators A*, 33, pp. 249-256, 1992.
11. M.C. Wu, L.Y. Lin, S.S. Lee, and K.S.J. Pister, "Micromachined Free-Space Integrated Micro-Optics," *Sensors and Actuators: A. Physical*, Vol. 50, No. 1-2, pp. 127-134, December 1995.
12. S.S. Lee, L.Y. Lin, and M.C. Wu, "Surface-Micromachined Free-Space Fiber Optic Switches," *Electronics Letters*, Vol. 31, No. 17, pp. 1481-1482, August 1995.
13. L.Y. Lin, S.S. Lee, K.S.J. Pister, and M.C. Wu, "Three-dimensional Micro-Fresnel Optical Elements Fabricated," *Micromachining Technique by Electronics Letters*, Vol. 30 No. 5
14. L.Y. Lin, S.S. Lee, K.S.J. Pister, and M.C. Wu, "Micro-Machined Three-Dimensional Micro-Optics for Integrated Free-Space Optical System," *IEEE Photonics Technology Letters*, Vol. 6, No. 12, December 1994.
15. A. Jazairy, N.C. MacDonald, Y.H. Lo, "Microelectromechanical Fabry-Perot Interferometer," 1995 Optical Society of America Annual Meeting, Sept. 10-15, 1995, Portland, Oregon, Paper WH4.
16. T.T.D. Tran, Y.H. Lo, A.H. Zhu, D. Haronian, E. Mozdy, "Surface micromachined Fabry-Perot tunable filter," *IEEE Photonics Tech. Lett.*, Vol. 8, no. 3, pp. 393-395, 1996.
17. E.C. Vail, M.S. Wu, G.S. Li, L. Eng, C.J. Chang-Hasnain, "GaAs micromachined widely tunable Fabry-Perot filters," *Elec. Lett.*, Vol. 31, no. 3, pp. 228-229, 1995.
18. L.Y. Lin, J.L. Shen, S.S. Lee, M.C. Wu, and A.M. Sergent, "Tunable three-dimensional solid Fabry-Perot etalons fabricated by surface-micromachining," *IEEE Photonics Tech. Lett.*, Vol. 8, no. 1, pp. 101-103, 1996.
19. J.L. Shen, L.Y. Lin, S.S. Lee, M.C. Wu, and A.M. Sergent, "Surface-micromachined tunable three-dimensional solid Fabry-Perot etalons with dielectric coatings," *Elec. Lett.*, Vol. 31, no. 25, pp. 2172-2173, 1995.
20. M.F. Dautartas, A.M. Benzoni, Y.C. Chen and G.E. Blonder, " A silicon-based moving-mirror optical switch", *J. of Lightwave Technology*, Vol. 10, No. 8, August, 1992.

21. S.S. Lee, L.Y. Lin, and M.C. Wu, "Surface-Micromachined Free-Space Fiber Optic Switches," *Electronics Letters*, Vol. 31, No. 17, pp. 1481-1482, August 1995.
22. P. Di Vita and U. Rossi, "Evaluation of coupling efficiency in joints between optical fibers", *Alta Frequenza*, Vol. XLVII, no. 7, pp. 414-423, 1978.
23. Devi S. Gunawan, and Lih-Yuan Lin, Kristofer S.J. Pister, "Micromachined Corner Cube Reflectors as a Communication Link." *Sensors and Actuators A* 46-47 (1995) 580-583.
24. L.J. Hornbeck, "Digital light processing and MEMS: Reflecting the digital display needs of the networked society," SPIE/EOS European Symposium on Lasers, Optics, and Vision for Productivity in Manufacturing I, Besancon, France, June 10-14, 1996. (invited paper).
25. R.L. Knipe, "Challenges of a digital micromirror device: Modeling and design," SPIE/EOS European Symposium on Lasers, Optics, and Vision for Productivity in Manufacturing, Besancon I, France, June 10-14, 1996.
26. L.J. Hornbeck, (invited paper) "Current status of the digital micromirror device (DMD) for projection television applications," *International Electron Devices Technical Digest*, pp. 381-384, 1993.
27. J.B. Sampsel, "An overview of the digital micromirror device (DMD) and its application to projection displays," *1993 SID International Symposium Digest of Technical Papers*, Vol 24, p.1012, 1993.
28. C. Tew et al., "Electronic control of a digital micromirror device for projection displays," *1994 IEEE Solid-State Circuits Digest of Technical Papers*, Vol. 37, p.130, 1994.
29. J. Younse, "Mirrors on a chip," *IEEE Spectrum*, Vol. 30, No. 11, p. 27, November 1993.
30. M.E. Motamedi, A.P. Andrews, W.J. Gunning, M. Khoshnevisan, "Miniaturized micro-optical scanners," *Optical Engineering*, Vol. 33, No. 11, pp. 3616-3623, Nov. 1994. (invited paper)